RSC Publishing Faraday Discussions

Exploring ligand-induced backdonation using X-ray spectroscopic methods

Journal:	*Faraday Discussions*
Manuscript ID	FD-ART-04-2019-000041.R1
Article Type:	Paper
Date Submitted by the Author:	04-Jun-2019
Complete List of Authors:	He, Weiying; The University of British Columbia, Chemistry Kennepohl, Pierre; The University of British Columbia, Chemistry

SCHOLARONE™
Manuscripts

ARTICLE

Direct experimental evaluation of ligand-induced backbonding in nickel metallacyclic complexes

Weiying He[a] and Pierre Kennepohl*[,a]

Received 00th January 20xx,
Accepted 00th January 20xx

DOI: 10.1039/x0xx00000x

The details of ligand-induced backbonding in nickel diphosphine π complexes are explored using nickel L-edge (3*d*←2*p*) x-ray absorption spectroscopy as a means of quantifying the degree of backbonding derived from direct Ni 3*d* donation into the π ligand. It is observed that backbonding into weakly π acidic ligands such as alkenes and arenes is dominated by contributions from the diphosphine ligand via σ-donation, leading to activated metallacycles with a Ni(0) d^{10} metal centre. With more strongly π acidic ligands, however, metal contributions to backbonding increase substantially leading to a more electron-deficient metal centre that is best described as having a Ni(I) spectroscopic oxidation state.

Introduction

Transition metal catalysed processes involving unsaturated organic substrates (e.g. alkenes, ketones, and other related species) often involves substrate activation via interactions between the metal centre and the π system. Bonding in such π adducts is commonly described using the framework first established by Dewar, Chatt, and Duncanson[1,2]. The DCD model focuses on the direct overlap of available π-type orbitals on the unsaturated ligand (π_b and π*) and valence metal *d* orbitals of appropriate symmetry (Figure 1), generating two primary interactions that contribute to bonding in such π adducts. One of these interactions involves σ donation from the ligand in an empty valence orbital on the metal (M*n*d←Lπ_b). The second interaction, commonly known as *π-backbonding*, involves π-type donation from the metal into an empty π* orbital on the ligand (M*n*d→Lπ*). The degree of π-backbonding is critical in defining the nature of the resultant organometallic complex. Two conceptual limiting cases can be defined based on the degree of backbonding (Figure 1): in the weakly backbonding limit, a weakly bound π-adduct is formed (M^nL), whereas in the strongly backbonding limit, the π bond in the ligand is broken via formal two-electron transfer from the metal to the ligand to form an $M^{n+2}X_2$-type metallacycle. Such π-type ligands are, therefore, redox-active two-electron reservoirs modulated and controlled by interactions with the metal centre.[3]

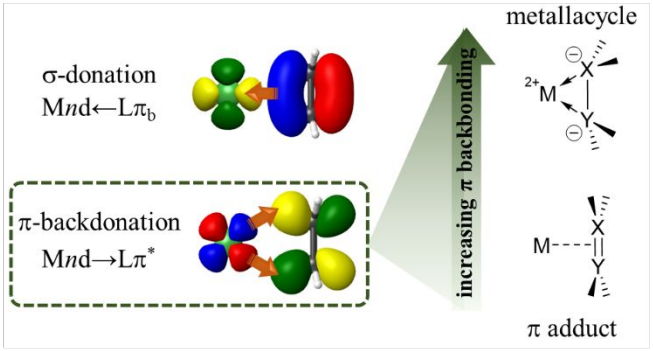

Figure 1 Fundamental metal-ligand interactions as defined in the classic Dewar-Chatt-Duncanson (DCD) model describing the bonding of alkenes with transition metal ions (left) and resulting limiting structures obtained based on the degree of backbonding (right).

Given the broad interest in nickel-catalysed cross-coupling strategies, and the proposed intermediacy of nickel π adducts in many such processes,[4–8] we recently probed the bonding in a series of nickel π adducts with diphosphine ancillary ligands[9], whose reactivity had been explored.[10–12] Our x-ray spectroscopic studies uncovered an intriguing scenario wherein weakly π acidic ligands such as alkenes and arenes are highly activated through backbonding whilst the metal centre is still extremely electron rich. In principle, these complexes defy the generalized predictions of the DCD bonding model by yielding Ni(0) metallacycles: the π bond in the alkene is essentially broken without concomitant oxidation of the metal centre. By contrast, more π acidic ligands show significant charge depletion at the metal centre leading to more Ni(I) character at the metal centre. This discovery was supported by complementary density functional theory (DFT) calculations, which provided a plausible rationale for our observations: activation of the π ligand was driven by donation from the ancillary diphosphine ligands via σ-donation through the formation of a formal 3-centre-4-electron (3c-4e) bond across

[a.] *Address here.*
[b.] *Address here.*
[c.] *Address here.*
† Footnotes relating to the title and/or authors should appear here.
Electronic Supplementary Information (ESI) available: [details of any supplementary information available should be included here]. See DOI: 10.1039/x0xx00000x

the equatorial plane of these planar complexes (Figure 2). The metal centre therefore mediates ligand-to-ligand charge donation the phosphines to the π ligand, a scenario which we have termed *ligand-induced backbonding*[13].

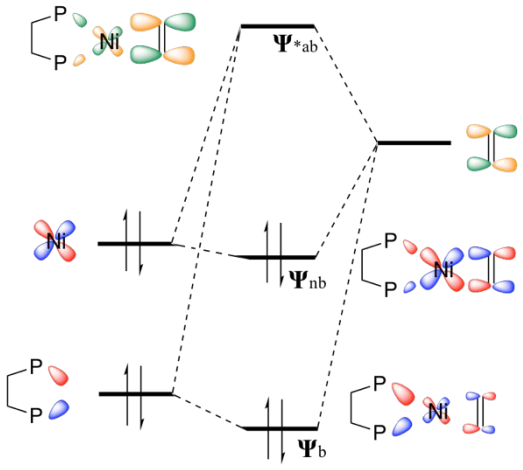

Figure 2 Molecular orbital representation of the 3c-4e bonding proposed for square planar Ni(0) diphosphine complexes with alkenes and other π ligands[8,9].

The specifics of this bonding model, albeit consistent with available experimental data, could not be directly probed with available spectroscopic measurements. For example, Ni K-edge x-ray absorption spectroscopy (XAS) is very effective as an experimental probe of the overall electron density at the metal centre in square planar nickel complexes given that the dominant (electric dipole allowed) pre-edge transition is dominated by Ni $4p_z \leftarrow 1s$ character; given the non-bonding character of this transition, it effectively reports on the overall charge at the metal centre. To evaluate the specifics of bonding in these complexes, contributions from 3*d* states must be probed. Unfortunately, $3d \leftarrow 1s$ transitions are electric dipole forbidden ($\Delta l = 2$) and thus extremely weak in metal K-edge spectra.[14,15] Ni $K_{\beta 1,3}$ x-ray emission spectroscopy (XES) involves core Ni $3p \rightarrow 1s$ transitions and is also somewhat insensitive to the specifics of bonding.[16]

Herein, we explore the details of bonding in representative nickel π complexes (Scheme 1) using Ni L-edge XAS to directly probe the occupancy of the Ni 3d orbitals and thus directly evaluate the Ni 3*d* orbital contributions to backbonding in such species. L-edge XAS of first-row transition metal complexes provides the opportunity to quantitatively evaluate the degree of covalency in metal-ligand bonds.[17] Such analyses have been most commonly utilized in the investigation of copper[18,19], and iron[20–23]complexes but the overall principles are applicable to any first-row transition metal complex, including nickel organometallics[24].Our analysis provides direct experimental support for the importance of ligand-induced backbonding in these complexes.

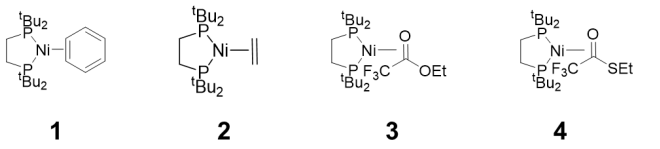

Scheme 1 Nickel complexes (**1**-**4**) investigated in this study. Previous investigations have suggested that **1** & **2** are best described as Ni(0) metallacycles, whereas **3** & **4** involve greater metal contributions to backdonation leading to greater Ni(I) character.

Results and Discussion

Experimental Ni $L_{3,2}$-edge XAS spectra for the ethylene (**1**) and arene (**2**) complexes (Figure 3A,B) exhibit very weak features in the near-edge region yet are more feature-rich than typically observed for d^{10} species.[25] Three features are clearly observable at the L_3 edge. The data for the more π acidic ester (**3**) and thioester (**4**) complexes (Figure 3C,D) show similar edge features shifted to higher energies (by ~1 eV) as well as an additional prominent shoulder at low energy. In all cases, the features observed at the L_2-edge are similar to those at the L_3-edge but are weaker and broader, as expected.[26]

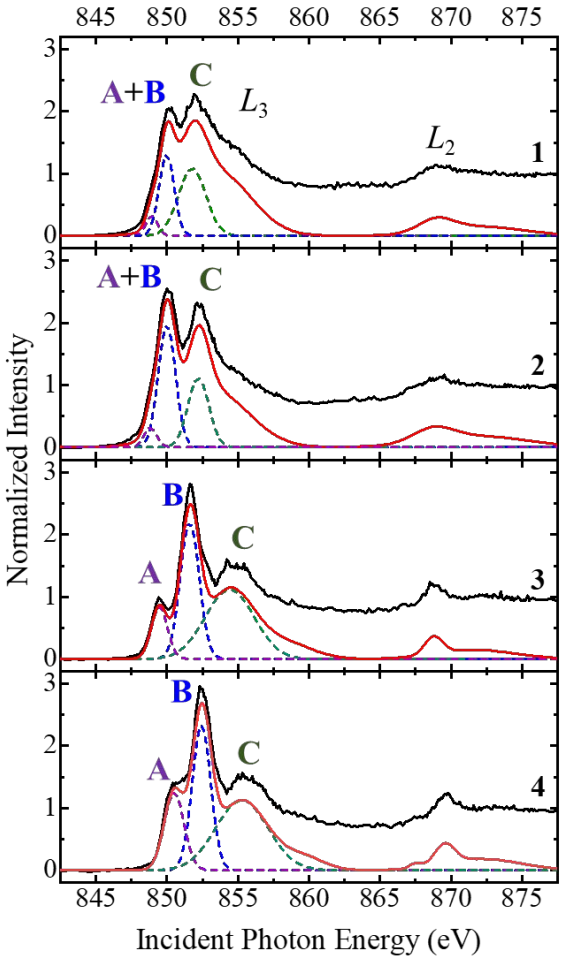

Figure 3 Normalized Ni $L_{3,2}$-edge XAS spectra for **1**-**4**. Experimental data are shown in black and the simulated spectra are shown in red (background removed for clarity).

This journal is © The Royal Society of Chemistry 20xx

Dashed lines are Gaussian functions represents each transition component (A-C). See details of simulation in SI 01-08

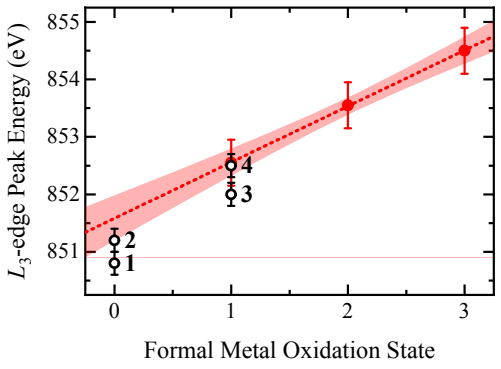

Figure 4 Intensity-weighted average energy of Ni L_3-edge spectroscopic features as a function of formal oxidation state. Reference data are taken from previous studies by Cramer and coworkers[29]. The red shaded area represents the 95% confidence interval from the Cramer data. Also plotted are the intensity-weighted average energies of the L3-edge features for complexes **1**-**4** in this work.

The energies of first-row transition metal L_3-edge features correlate very well with oxidation states[27,28]. The literature on Ni *L*-edges is somewhat sparse, but Cramer and coworkers have demonstrated this relationship for Ni(I), Ni(II), and Ni(III) species[29,30].Linear extrapolation of these data suggests that L_3-edge spectra of molecular Ni(0) species should centre at ~851.5 eV, in good agreement with our experimental data for **1** & **2**. The shift to higher energy for the main features of **3** & **4** by ~1 eV is consistent with a spectroscopic oxidation state of Ni(I) based on this correlation (see Figure 4).

The high *d* occupancy in these species dramatically simplifies analysis of the L-edge spectra and allows for reasonable modelling of the final states without invoking atomic multiplets from multielectron configurational states[22,31]. Time-dependent DFT (TD-DFT) calculations are therefore useful for evaluating the most important contributions to the spectra[25]. TD-DFT simulations of the Ni L-edges using B3LYP/def2-TZVP with zero-order relativistic corrections as implemented in ORCA 4.0 are shown in Figure 5; these results qualitatively mirror those of the experimental Ni L_3-edges. A summary of the relevant TD-DFT calculated final states for each of the complexes are given in Table 1.

The nature of the final states listed in Table 1 is similar to that obtained for Ni K-edges[9], although relative contributions from each of these final states is very different due to differences in the initial state. Simulated spectra for **1** & **2** predict two important features - in good agreement with the experimental data. The lowest energy feature results from two contributions: (*i*) the ligand acceptor π* orbital involved in backbonding (Lπ* ← Ni2p), and (*ii*) a Ni 4p_z shakedown with significant diphosphine ligand character (Ni4p + LMCT ← Ni2p). The Ni 4p_z final state gains intensity from mixing with dipole-allowed Ni 3*d* orbital character. The total intensity of this feature represents the overall depletion of electron density from the 3*d* manifold both to higher lying metal states (via hybridization) and backdonation to the ligands. By contrast, the intensity of the higher energy feature is dominated by Ni 4*s* contributions in ligand-based final states; this dipole-allowed Ni 4*s* ← Ni 2*p* (|Δ*l*| = 1) feature is not observed in the corresponding Ni K-edge spectra as they correspond to an electric dipole forbidden Ni 4*s* ← Ni 1*s* (|Δ*l*| = 0). This feature includes only minor Ni 3*d* contributions and therefore the intensity of this feature does not reflect 3*d* electron depletion. A broad shoulder at higher energy is also observed and is attributed to more ill-defined Rydberg final states[32]. The shifts to higher energy and the appearance of a low energy shoulder in the experimental spectra of **3** & **4** (relative to **1** & **2**) also occur in the simulated spectra of these species. The simulations indicate similar transitions as those observed in **1** & **2** but with systematic changes as summarized in Figure 6. Final states with significant Ni 4*s* and 4*p* contributions (**C** & **B**, respectively) shift to higher energy, in accordance with a decrease in the electron density at the metal centre. The energy of the Lπ* final states (**A**), *i.e.*, those involved in backbonding, are lower in energy for these species because of the inherently greater π acidity of the ligands in these complexes. The intensity of the feature A increases as a function of the π acidity of the ligand, which reflects an increase in the contribution from the Ni 3d manifold in these Lπ* final states. The change is substantial on going from alkene/arene ligands (~10% for **1**/**2**) to the electron poor ester/thioester (~25% for **3**/**4**).

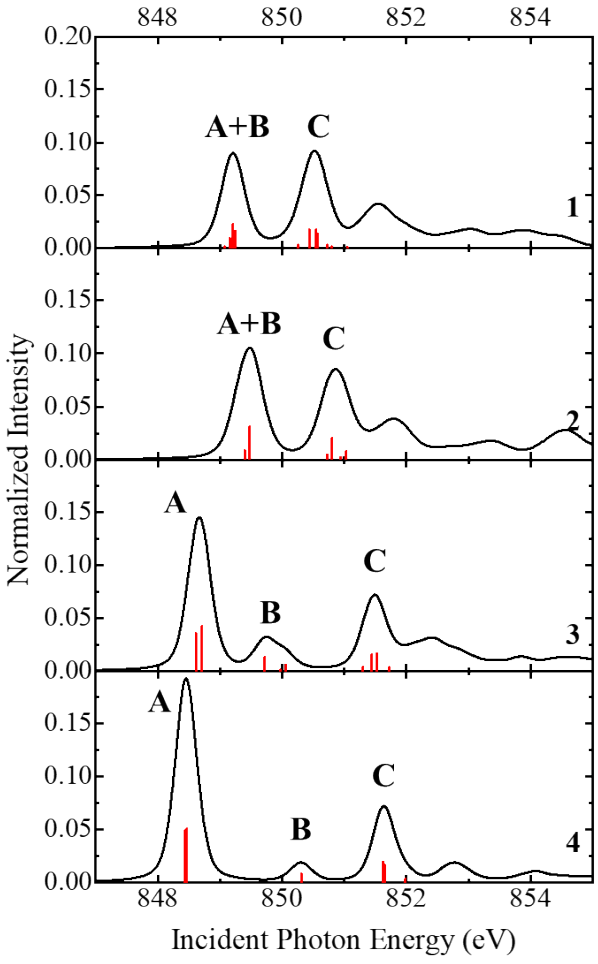

Figure 5 TD-DFT calculated Ni L-edge XAS spectrum for **1**-**4**. Overall simulated spectra are obtained by including an arbitrary isotropic broadening (FWHM = 0.05 eV) to the sum of all individual contributing final states. Drop lines (red) indicate the dominant contributing final states to the overall simulated spectrum. The details of each of these final states is given in Table 1.

The experimental and simulated *L*-edges are in agreement with the conclusion that Ni 3*d* charge depletion is small in both **1** and **2** even though the π ligands are strongly activated through significant backbonding.[9] This observation supports the predominance of *ligand-induced backbonding*, which allows for π backbonding from the ancillary diphosphine ligand to the π ligand with only minimal contributions from the metal. Although quantitative evaluation of covalency has been performed for other transition metals such as copper and iron, appropriate validated references are not currently available for nickel complexes. However, the relative intensities of the contributing features in the L-edge spectra may be used to evaluate the changes in the metal contributions to backbonding in each of the complexes.

Complex	Peak	E_{avg}	I_{tot}	% Ni (3d)	% L	% dtpe	final state
1	A	849.2	0.039	20 (14)	39	41	Lπ^* + 3d_{x2-y2}
	B	849.1	0.011	31 (6)	24	45	dtpe + Ni 4p_z
	C	850.5	0.053	10 (2)	15	75	dtpe + Ni 4*s*
2	A	849.5	0.056	7 (5)	31	63	Lπ^* + 3d_{x2-y2}
	B	849.4	0.009	13 (3)	5	82	dtpe + Ni 4*pd*
	C	850.9	0.036	5 (1)	5	90	dtpe + Ni 4*s*
3	A	848.7	0.078	28 (26)	33	38	Lπ^* + 3d_{x2-y2}
	B	849.8	0.021	43 (7)	17	40	dtpe + Ni 4p_z
	C	851.5	0.041	8 (2)	4	88	dtpe + Ni 4*s*
4	A	848.5	0.100	34 (25)	31	35	Lπ^* + 3d_{x2-y2}
	B	851.4	0.045	20 (8)	6	74	dtpe + Ni 4p_z
	C	852.0	0.003	6 (1)	0	94	dtpe + Ni 4*s*

Table 1 Summary of TD-DFT calculated Ni L-edge XAS data for **1**-**4**. Each row represents a family of transitions (with an average energy, E_{avg}, and a total intensity, I_{tot}). Each of these families of transitions are ascribed to particular features in the Ni L_3-edge spectra (**A**, **B**, and **C** in Figures 3 & 5). The averaged distribution of the final state acceptor orbitals is also broken down between the metal (Ni, metal 3*d* contributions given in parentheses), the π ligand (L), and the diphosphine ligand (dtpe). A detailed breakdown of all relevant TD-DFT calculated transitions are given in supplementary Information SI09-20.

As noted previously, there are two mechanisms for Ni 3*d* contributions to bonding in these species; each of these is reflected in the Ni L_3-edge spectra. Peak **A** derives intensity from direct Ni 3*d* contributions to backbonding, whereas the intensity of peak **B** reflects Ni 3*d*/4*p* mixing. We note that the overall Ni 3*d* contributions to bonding correlate very well with the energy of the Ni 4*p*←1*s* transition (see supporting information, SI21), which reflects spectroscopic oxidation states. For both the alkene and arene complexes, Ni 3*d* contributions are relatively small such that **1** & **2** are best described as *Ni(0) metallacycles*. This formulation is atypical within the DCD bonding model, which envisages the formation of metallacycles with concomitant two-electron oxidation of the metal centre (i.e., a Ni(II) metallacycle). Formal cleavage of the C=C π bond is achieved primarily through charge donation from the diphosphine ligands rather than the metal centre.(ref) In more π acidic systems such as **3** & **4**, the metal contribution to backbonding increases relative to that of the diphosphine (Figure 6), resulting in formal metal oxidation. These complexes have a more Ni(I)-like electronic configuration via increased covalency. Although ligand contributions are still extremely importantly in such species, metal donation is significant. We anticipate that the reactivity of complexes with dominant *ligand-induced backbonding* such as **1** & **2**, where metal contributions are very small, will differ markedly from those with more classical metal-based backbonding. We postulate that this may be an important factor in reactivity differences between nickel and its noble metal analogs, palladium and platinum, for whom metal-based backbonding is known to be very important.[33]

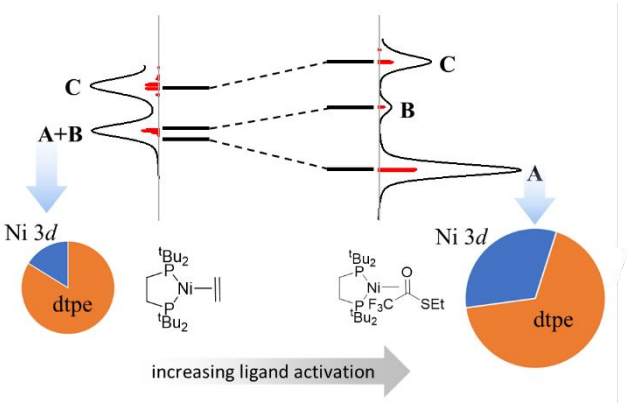

Figure 6 Schematic representation of changes in final states between **2** (left) and **4** (right). Most final states (**B**, **C** - see Table 1 for details) increase in energy due to charge depletion at the metal centre except for Lπ* states (**A**), which decreases in energy and increases in intensity. These changes occur because of increased charge donation from the metal centre in response to greater π acidity in the ligand. Each pie chart represents the changes in Ni and dtpe charge donation from to the π ligand for each of the complexes. The Ni 3d contribution to backbonding increases from under 20% to ~35% between the two complexes.

Conclusions

Nickel $L_{3,2}$-edge spectroscopic data on a series of well defined nickel diphosphine π complexes to provide support for the critical role of *ligand-induced backbonding* in bond formation and ligand activation. The data and supporting computational data indicate two major sources of Ni 3*d* contributions to bonding and a direct correlation between the degree of Ni 3*d* charge depletion and the spectroscopic oxidation state of the metal. In weakly π acidic complexes, Ni 3*d* contributions are very small even though the π ligand is strongly activated. With more strongly π acidic ligands, contributions from the metal increase leading to partial oxidation of the metal centre. These results support a direct involvement of ancillary ligands in π

This journal is © The Royal Society of Chemistry 20xx

backbonding. The implications for reactivity are still being elucidated.

Experimental

Sample Preparation Selected (dtbpe)Ni (dtbpe = 1,2-bis(di-*tert*-butyl)phosphino)ethane) π-complexes were prepared as previously described.[10–12]

Spectroscopic Measurements XAS spectra were recorded at beamline 10-1 at the Stanford Synchrotron Radiation Lightsource (SSRL). Total electron yield (TEY) detection was used for the acquisition of Ni L-edge spectra between 840–960 eV with a channeltron electron multiplier. The incident beam intensity was monitored via a gold grid and used as I_0 to normalize the total electron yield signal I_1. For comparison, the normalized (I_1/I_0) spectra were renormalized to each other's maximum. The scans were recorded with a step size of 0.3 eV and an integration time of 1 s/pt. The energy resolution of the incident radiation is ~0.3 eV. Each final spectrum was the sum of five scans from different sample spots. Energy calibration was performed using NiF_2 , with an L_3-edge feature at 852.7 eV.[34] The incident angle was set at 55° with respect to the sample surface. All samples were measured at room temperature. To minimize radiation damage, a defocused beam (about 1×1 mm^2) was used.

Computational methods Initial geometries for all molecules were obtained from crystallographic coordinates (where available) or constructed from standard models. Geometry optimizations and numerical frequency calculations were performed using version 4.0 of the ORCA computational chemistry package[35]. Molecular geometries were optimized using the B3LYP functional in combination with the Ahlrichs triple-ζ basis set with valence polarization (def2-TZVP) for all atoms. Computational efficiency was improved by applying the RI approximation (RIJCOSX) for the hybrid functional[19]. All calculations were performed with integration grid 4. Reported thermochemical energies are given in kJ/mol and correspond to Gibbs free energies (ΔG^0) with zero-point vibrational energy corrections (ZPVE). All calculations were run on either the Abacus (UBC Chemistry) or GREX (Westgrid) computing clusters.

Conflicts of interest

There are no conflicts to declare.

Acknowledgements

This work is supported by the Natural Sciences and Engineering Research Council (NSERC) Canada through a Discovery Grant to PK. WH is grateful to Mitacs Canada for a Globalink Graduate Fellowship. We also thank for Charles J. Titus for assistance in performing experiments at beamline 10-1. Use of the Stanford Synchrotron Radiation Lightsource, SLAC National Accelerator Laboratory, is supported by the U.S. Department of Energy, Office of Science, Office of Basic Energy Sciences under Contract No. DE-AC02-76SF00515. The SSRL Structural Molecular Biology Program is supported by the DOE Office of Biological and Environmental Research, and by the National Institutes of Health, National Institute of General Medical Sciences (including P41GM103393). The contents of this publication are solely the responsibility of the authors and do not necessarily represent the official views of NIGMS or NIH.

Notes and references

1 G. Frenking, *J. Organomet. Chem.*, 2001, **635**, 9–23.
2 J. Chatt and L. A. Duncanson, *J. Chem. Soc.*, 1953, **0**, 2939.
3 A. N. Desnoyer, S. Behyan, B. O. Patrick, A. Dauth, J. A. Love and P. Kennepohl, *Inorg. Chem.*, 2016, **55**, 13–15.
4 W. Guo, C. Michel, R. Schwiedernoch, R. Wischert, X. Xu and P. Sautet, *Organometallics*, 2014, **33**, 6369–6380.
5 Y. Hoshimoto, M. Ohashi and S. Ogoshi, *J. Am. Chem. Soc.*, 2011, **133**, 4668–4671.
6 Y. Kita, R. D. Kavthe, H. Oda and K. Mashima, *Angew. Chemie Int. Ed.*, 2016, **55**, 1098–1101.
7 D. K. Nielsen and A. G. Doyle, *Angew. Chemie Int. Ed.*, 2011, **50**, 6056–6059.
8 W. He, B. O. Patrick and P. Kennepohl, *Nat. Commun.*, 2018, **9**, 3866.
9 A. Desnoyer, W. He, P. Kennepohl, S. Behyan, W. Chiu, J. A. Love and A. Desnoyer, *Chem. - A Eur. J.*, , DOI:10.1002/chem.201805987.
10 A. N. Desnoyer, W. Chiu, C. Cheung, B. O. Patrick and J. A. Love, *Chem. Commun.*, 2017, **53**, 12442–12445.
11 A. N. Desnoyer, F. W. Friese, W. Chiu, M. W. Drover, B. O. Patrick and J. A. Love, *Chem. - A Eur. J.*, 2016, **22**, 4070–4077.
12 A. N. Desnoyer, E. G. Bowes, B. O. Patrick and J. A. Love, *J. Am. Chem. Soc.*, 2015, **137**, 12748–12751.
13 A. Stockis and R. Hoffmann, *J. Am. Chem. Soc.*, 1980, **102**, 2952–2962.
14 J. L. DuBois, P. Mukherjee, A. M. Colier, J. M. Mayer, E. I. Solomon, B. Hedman, T. D. P. Stack and K. O. Hodgson, *J. Am. Chem. Soc.*, 1997, **119**, 8578–8579.
15 T. E. Westre, P. Kennepohl, J. G. DeWitt, B. Hedman, K. O. Hodgson and E. I. Solomon, *J. Am. Chem. Soc.*, 1997, **119**, 6297–6314.
16 N. Lee, T. Petrenko, U. Bergmann, F. Neese and S. Debeer, *J. Am. Chem. Soc.*, 2010, **132**, 9715–9727.
17 Y. Ha, A. R. Arnold, N. N. Nuñez, P. L. Bartels, A. Zhou, S. S. David, J. K. Barton, B. Hedman, K. O. Hodgson and E. I. Solomon, *J. Am. Chem. Soc.*, 2017, **139**, 11434–11442.
18 R. Sarangi, N. Aboelella, K. Fujisawa, W. B. Tolman, B. Hedman, K. O. Hodgson and E. I. Solomon, *J. Am. Chem. Soc.*, 2006, **128**, 8286–8296.
19 R. C. Walroth, K. C. Miles, J. T. Lukens, S. N. MacMillan, S. S. Stahl and K. M. Lancaster, *J. Am. Chem. Soc.*, 2017, **139**, 13507–13517.
20 R. K. Hocking, E. C. Wasinger, Y. L. Yan, F. M. F. Degroot, F. A. Walker, K. O. Hodgson, B. Hedman and E. I. Solomon, *J. Am. Chem. Soc.*, 2007, **129**, 113–125.
21 R. K. Hocking, S. D. George, K. N. Raymond, K. O. Hodgson, B. Hedman and E. I. Solomon, *J. Am. Chem. Soc.*, 2010, **132**, 4006–4015.
22 R. K. Hocking, E. C. Wasinger, F. M. F. de Groot, K. O. Hodgson, B. Hedman and E. I. Solomon, *J. Am. Chem. Soc.*, 2006, **128**, 10442–10451.
23 E. C. Wasinger, F. M. F. De Groot, B. Hedman, K. O. Hodgson and E. I. Solomon, *J. Am. Chem. Soc.*, 2003, **125**, 12894–12906.
24 S. L. Hulbert, B. A. Bunker, F. C. Brown and P. Pianetta, *Phys. Rev. B*, 1984, **30**, 2120–2126.

25 R. C. Walroth, J. T. Lukens, S. N. MacMillan, K. D. Finkelstein and K. M. Lancaster, *J. Am. Chem. Soc.*, 2016, **138**, 1922–1931.
26 A. L. Ankudinov, A. I. Nesvizhskii and J. J. Rehr, *Phys. Rev. B - Condens. Matter Mater. Phys.*, 2003, **67**, 6.
27 P. A. Van Aken, B. Liebscher and V. J. Styrsa, *Phys. Chem. Miner.*, 1998, **25**, 323–327.
28 L. A. J. Garvie and P. R. Buseck, *Nature*, 1998, **396**, 667–670.
29 H. Wang, D. S. Patil, W. Gu, L. Jacquamet, S. Friedrich, T. Funk and S. P. Cramer, *J. Electron Spectros. Relat. Phenomena*, 2001, **114–116**, 855–863.
30 H. Wang, C. Y. Ralston, D. S. Patil, R. M. Jones, W. Gu, M. Verhagen, M. Adams, P. Ge, C. Riordan, C. A. Marganian, P. Mascharak, J. Kovacs, C. G. Miller, T. J. Collins, S. Brooker, P. D. Croucher, K. Wang, E. I. Stiefel and S. P. Cramer, *J. Am. Chem. Soc.*, 2000, **122**, 10544–10552.
31 M. L. Baker, M. W. Mara, J. J. Yan, K. O. Hodgson, B. Hedman and E. I. Solomon, *Coord. Chem. Rev.*, 2017, 345, 182–208.
32 U. Bergmann, P. Glatzel and S. P. Cramer, *Microchem. J.*, 2002, **71**, 221–230.
33 C. Liu, H. Zhang, W. Shi and A. Lei, *Chem. Rev.*, 2011, **111**, 1780–1824.
34 P. Olalde-Velasco, J. Jiménez-Mier, J. Denlinger and W.-L. Yang, *Phys. Rev. B*, 2013, **87**, 245136.
35 F. Wennmohs, D. Aravena, M. Atanasov, U. Becker, D. Bykov, V. G. Chilkuri, D. Datta, A. Kumar Dutta, D. Ganyushin, Y. Guo, A. Hansen, L. Huntington, R. Izsák, C. Kollmar, S. Kossmann, M. Krupička, D. Lenk, D. G. Liakos, D. Manganas, D. A. Pantazis, T. Petrenko, P. Pinski, C. Reimann, M. Retegan, C. Riplinger, T. Risthaus, M. Roemelt, M. Saitow, B. Sandhöfer, I. Schapiro, K. Sivalingam, G. Stoychev, B. Wezisla, M. Kállay, S. Grimme, E. Valeev, G. Chan, J. Pittner, M. Brehm, G. Bistoni and W. Schneider, *ORCA-An ab initio, DFT and semiempirical SCF-MO package-Version 4.0.1*.

This journal is © The Royal Society of Chemistry 20xx

Please do not adjust margins